Journal of Biomedical Optics

SPIEDigitalLibrary.org/jbo

Application of a time-resolved optical brain imager for monitoring cerebral oxygenation during carotid surgery

Michal Kacprzak
Adam Liebert
Walerian Staszkiewicz
Andrzej Gabrusiewicz
Piotr Sawosz
Grzegorz Madycki
Roman Maniewski

SPIE

Application of a time-resolved optical brain imager for monitoring cerebral oxygenation during carotid surgery

Michal Kacprzak,[a] Adam Liebert,[a] Walerian Staszkiewicz,[b] Andrzej Gabrusiewicz,[b] Piotr Sawosz,[a] Grzegorz Madycki,[b] and Roman Maniewski[a]
[a]Nalecz Institute of Biocybernetics and Biomedical Engineering PAS, Trojdena 4, 02-109 Warsaw, Poland
[b]Centre for Postgraduate Medical Education, Department of Vascular Surgery and Angiology, Marymoncka 99/103, 01-813 Warsaw, Poland

Abstract. Recent studies have shown that time-resolved optical measurements of the head can estimate changes in the absorption coefficient with depth discrimination. Thus, changes in tissue oxygenation, which are specific to intracranial tissues, can be assessed using this advanced technique, and this method allows us to avoid the influence of changes to extracerebral tissue oxygenation on the measured signals. We report the results of time-resolved optical imaging that was carried out during carotid endarterectomy. This surgery remains the "gold standard" treatment for carotid stenosis, and intraoperative brain oxygenation monitoring may improve the safety of this procedure. A time-resolved optical imager was utilized within the operating theater. This instrument allows for the simultaneous acquisition of 32 distributions of the time-of-flight of photons at two wavelengths on both hemispheres. Analysis of the statistical moments of the measured distributions of the time-of-flight of photons was applied for estimating changes in the absorption coefficient as a function of depth. Time courses of changes in oxy- and deoxyhemoglobin of the extra- and intracerebral compartments during cross-clamping of the carotid arteries were obtained. A decrease in the oxyhemoglobin concentration and an increase in the deoxyhemoglobin concentrations were observed in a large area of the head. Large changes were observed in the hemisphere ipsilateral to the site of clamped carotid arteries. Smaller amplitude changes were noted at the contralateral site. We also found that changes in the hemoglobin signals, as estimated from intracerebral tissue, are very sensitive to clamping of the internal carotid artery, whereas its sensitivity to clamping of the external carotid artery is limited. We concluded that intraoperative multichannel measurements allow for imaging of brain tissue hemodynamics. However, when monitoring the brain during carotid surgery, a single-channel measurement may be sufficient.
 [DOI: 10.1117/1.JBO.17.1.016002]

Keywords: time-resolved imaging; light propagation in tissues; medical optics instrumentation.

Paper 11334 received Jun. 30, 2011; revised manuscript received Oct. 28, 2011; accepted for publication Nov. 2, 2011; published online Feb. 8, 2012.

1 Introduction

Carotid endarterectomy is a surgical procedure that removes arteriosclerotic plaques from carotid arteries. The surgery is a relatively safe and effective intervention for reducing the risk of stroke[1–3] that is offered to patients with high-grade carotid stenosis. The surgery is carried out after clamping the carotid artery, which may cause hypoxia of the brain tissue. Temporal intraluminal shunts may be used to reduce the risk of perioperative stroke. Intraoperative monitoring of brain perfusion is essential for effective outcomes following this procedure, provided enough information on the necessity of shunt installation and the potential occurrence of watershed infarction following the surgical procedure is obtained.[4]

Rapid development of new brain imaging modalities has occurred over the last two decades. Methods like computed tomography,[5] diffusion-weighted MRI,[6,7] quantitative brain perfusion by single-photon emission computed tomography,[8] and transcranial Doppler ultrasound techniques[9] have been applied pre- and/or postoperatively and may be useful for the prevention and detection of postsurgical complications in the brain. However, most of the imaging methods available for clinical use require transportation of the patient to the imaging facility and cannot be used in the operative theater.

When carotid arteries are clamped, the reduction in the blood velocity can be intraoperatively monitored in the middle cerebral artery by the transcranial Doppler ultrasound technique (TCD).[10] This method may be used to control the effectiveness of intraoperative shunts. However, considerable skill and experience are necessary to carry out this technique and interpret the obtained intracranial sonograms. Moreover, this measurement cannot be carried out in about 10% of patients because of insonation is impossible of intracranial due to the thickness and density of the temporal bone.

Electroencephalography[11,12] or the monitoring of somatosensory-evoked potentials[13–16] may also be used for intraoperative monitoring of the neurological consequences of carotid artery clamping.

The third technique considered for monitoring brain tissue during carotid surgery is near-infrared spectroscopy. Near-infrared spectroscopy (NIRS)[17,18] is an optical technique with good potential for the bedside assessment of brain oxygenation.[19,20] The method evaluates changes in oxy- and deoxyhemoglobin, which can reveal different spectral properties in the near-infrared range of wavelengths.[21] The small size of

Address all correspondence to: Michal Kacprzak, Nalecz Institute of Biocybernetics and Biomedical Engineering PAS, Trojdena 4, 02-109 Warsaw, Poland. Tel: 00486599143 ext117; E-mail: mkacprzak@ibib.waw.pl

0091-3286/2012/$25.00 © 2012 SPIE

the instrumentation and its compatibility with biomedical monitoring devices also allows this technique to be used intraoperatively.

Classical NIRS measurements are carried out by fixing a source and detecting fibers or fiber bundles on the surface of the head and analyzing changes in the attenuation of the detected light. Source-detector separation is typically in the range of 2 to 4 cm. These changes in the attenuation of light are measured at several wavelengths and can be used to calculate changes in oxy- and deoxyhemoglobin. A distinct drawback of this technique, called continuous wave NIRS (cwNIRS), is connected with the fact that the measured brain oxygenation signals are contaminated by changes in the oxygenation of the extracerebral tissue. Measurement at several source-detector separations can be employed for improved differentiation of the signal originating from the brain.[22–24] In addition, two other modern optoelectronic techniques can be employed for this purpose. The first is the frequency-domain method in which the light that is shone onto a tissue is modulated at a high frequency. The phase shift between the emitted light wave and optical signal that is detected after penetration into the tissue is related to the path length of the photons between the source and the detector.[25–27] The second methods, which is the more sophisticated optical technique, is based on the emission of short (typically picosecond) laser pulses into the tissue and analysis of the broadening of these pulses during penetration into the tissue.[28,29] This technique is expensive and technically advanced, but potentially allows for the differentiation of information originating from the brain and extracerebral tissue layers.[22,30] In the present study, we show how the advantages of the time-resolved optical measurements can be utilized to evaluate brain oxygenation changes during carotid artery clamping following carotid endarterectomy.

NIRS techniques were already intensively tested as monitoring tools for brain assessment during carotid endarterectomy[31,32] In several studies, the authors have shown the usefulness of the NIRS technique[33–49] and they compared the effectiveness of this technique with transcranial Doppler sonography,[7,34,38,40,45,50] EEG measurement,[7,36,39,44] and the measurement of carotid artery stump pressure[39,48] for the prediction of the ischemic consequences of carotid endarterectomy. Recently, the NIRS technique has been extended to imaging, successfully applied during carotid endarterectomy, and shown preliminary potential for the detection of localized watershed infarction.[43]

A review of the NIRS validation studies was published and suggests that the method is potentially interesting.[31] The published study indicates the possible benefits of the NIRS technique utilization. However, the acceptance of this modality for the routine monitoring of patients undergoing carotid arteries endarterectomy needs studies that are carried out on large cohorts of patients. Moreover, the instruments offered by different manufacturers are not standardized and the signal-processing algorithms used may differ significantly. These instrumental discrepancies represent a serious obstacle for comparing results obtained by different clinical groups.

This phase of NIRS development is not finished and new, very sophisticated optical techniques (i.e., frequency-domain and time-resolved methods) have been introduced to measure brain oxygenation. However, up to now, these techniques were not applied for monitoring changes in brain oxygenation following carotid surgery. For the first time, we applied the time-resolved NIRS (trNIRS) technique for monitoring the brain during a carotid endarterectomy. The instrument was equipped with multiple source-detector pairs that were distributed on the head surface. This technique allowed us to image changes in tissue oxygenation with improved depth discrimination over a large area of investigated tissue.

2 Methods

2.1 *Instrumentation*

Experiments were carried out using our selfconstructed, time-resolved optical imager during carotid endarterectomy (Fig. 1). Our setup allows us to simultaneously assess changes in oxy and deoxyhemoglobin with depth discrimination by using 32 source-detector pairs located on the head (see Fig. 1).

The measurement method is based on the emission of picoseconds-long laser pulses into the brain tissue and the analysis of the temporal broadening of the reemitted light pulses using time-correlated single-photon counting (TCSPC) electronics. The light pulses from two laser diodes were controlled using Sepia PDL 808 (PicoQuant, Germany) were sequentially delivered to 18 points on the surface of the patient's head using two fast optomechanical fiber switches (1×9; Piezosystem Jena, Germany). The switching frequency was 10 Hz. To detect the reemitted light from the tissue, eight fiber bundles measuring 4-mm in diameter were used (Loptek, Germany). The source fibers and the detecting fiber bundles were placed on the head surface and they formed a 4×4 emitter-detector grid on each hemisphere, as shown in Fig. 1. The sourcedetector distance was fixed to 3 cm using a holder constructed of a thermoplastic material and soft rubber foam, which provided a good fit between the holder and the head. Eight photomultiplier tubes (R7400U-02; Hamamatsu Photonics, Japan) were used for detection of the diffusely reflected light at the 32 source-detector pairs. Eight independent TCSPC PCI boards (SPC-134; Becker & Hickl, Germany) were used for the acquisition of the distributions of the times of flight of the photons (DTOFs).

The instrumental response function (IRF) was measured by positioning the source fibers in front of the detecting bundles. The detecting bundles were covered with a sheet of white paper in order to fill up the whole numerical aperture of the bundle.[51] IRF of every source-detector pair was measured at both wavelengths, which was not longer than 800 ps (full width at half maximum, FWHM), and was in the range described by other studies on adult brains.[52,53] The width of the IRF depends on the laser pulse width and dispersion of light propagation from the emitting fibers. However, most important factor regarding the IRF width is the length and numerical aperture of the detecting fiber bundles and temporal response of the detectors being used. Considering the short distance between the output face of the detecting fiber bundle and the detector (less than 10 mm), the numerical aperture of the detecting system is large which leads to a high efficiency of photon detection. Under such conditions, a trade-off between the number of collected photons and width of the IRF is reached. It should be noted that even for the IRF width used in our time-resolved optical system (800 ps), rapid changes in the absorption coefficient of the brain tissue can be assessed because the stability of the IRF is most important for the proposed analysis of the measured DTOFs.

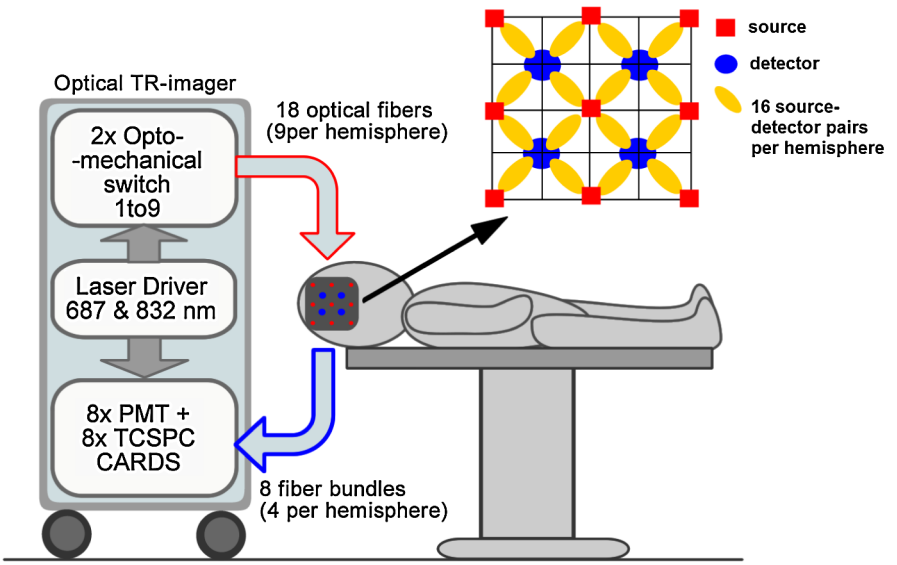

Fig. 1 The timeresolved optical imager used for intraoperative measurements. This setup is controlled by an industrial computer and consists of a laser driver with 2-ps laser diodes operating at wavelengths of 687 nm and 832 nm. Two optomechanical fiber switches deliver the light to the surface of the head. The diffusely reflected light is collected by the fiber bundles and eight independent time-correlated single-photon counting (TCSPC) channels with the photomultiplier tubes (PMT). The laser driver triggers the diodes with an 80-MHz frequency and sends the synchronization signal to the TCSPC electronics. Data from 32 source-detector pairs, forming a 4×4 array on each hemisphere, are recorded at a frequency of 1 Hz.

The holder of the optical fibers and optical fiber bundles was specially designed for application to the surface of the head by hand. The assistant fixes the holder by hand in such a position that the middle of each optode setup is located above the C3 and C4 points (according to the specification of a 10–20 EEG system). Thus, the measurement area is able to cover the motor cortex region of the brain.

2.2 *Patients and Operating Procedure*

A group of 16 patients with atherosclerotic disease was monitored by the trNIRS method during routine carotid endarterectomy surgery at the Department of Vascular Surgery and Angiology, Centre for Postgraduate Medical Education, Warsaw, Poland.[3,32] Eleven males and 5 females with a mean age of 73 years, ranging from 54 to 87 years, were examined. During the whole measurement campaign, 6 left and 10 right carotid arteries were operated on. This research was approved by the hospital's ethics committee.

During the measurements, the patients were horizontally positioned with the head fixed to the operating table. A dark curtain, which isolated the fiber holder from external light sources, was placed next to the patient's head. During the whole endarterectomy procedure, the patients were conscious the entire time in order to observe neurological reactions caused by cross-clamping of the carotid arteries. A local anesthesia was introduced at the neck. The patient's head was rotated about 30 deg in order to expose the operating field. The fiber holder was fixed to the head only during the crossclamping of the carotid arteries. Each stage of the surgery was announced by the surgeon and marked as an event in the data log. After the arteries were prepared, the clamps were fixed to the external carotid artery (ECA), common carotid artery (CCA), and internal carotid artery (ICA). Then, the cross-camping procedure was performed and the patient was carefully observed in order to evaluate the clinical symptoms of ischemia.

The crossclamping procedure of each artery was carried out in the following order (Fig. 2): first, the ECA was occluded, after approximately 4 s, the CCA and then the ICA were occluded. The time between the occlusion of the CCA and ICA was usually less than 1 s. Thus, it was assumed that the time of CCA occlusion was identical to the time of ICA occlusion. The proper order of cross-clamping is essential for the prevention of microembolization. In the case of loss of consciousness or other neurological deficit, the intraluminal shunt was inserted, the selected artery was opened, and the atherosclerotic plaque was carefully removed. The duration of cross-clamping the carotid arteries was between 12 and 26 min. After the carotid plaques were removed, restoration of blood flow was performed in the following manner: first in the ECA, then the CCA, and, finally, the ICA. This order is very important in order to prevent

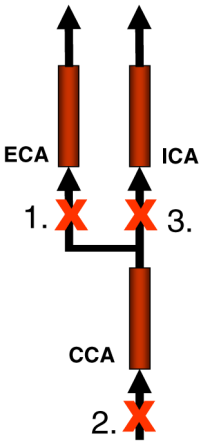

Fig. 2 Stages of crossclamping the carotid arteries during carotid endarterectomy. (1) Crossclamping of the external carotid artery (ECA). (2) Crossclamping of the common carotid artery (CCA). (3) Crossclamping of the internal carotid artery (ICA).

transpositions of small atherosclerotic particles from the blood stream into intracerebral circulation.

2.3 *Data Analysis*

The main goal of utilizing a time-resolved imaging system during carotid artery endarterectomy is to assess changes in oxyhemoglobin (ΔHbO_2) and deoxyhemoglobin (ΔHb) concentrations with depth discrimination. For this purpose, we applied a procedure based on the analysis of the statistical moments of the distributions of time of flight of photons and their sensitivity factors that have been previously described.[22,54] We considered three statistical moments of the DTOFs: N_{tot}, the total number of photons (zero-order, non-normalized moment integral); $\langle t \rangle$, the mean time of flight of photons (first moment); and V, the variance of the DTOF (second-centralized moment).

The human head under investigation is an inhomogeneous medium and represents a layered structure. In such a multilayered model, we can distinguish two main compartments: extracerebral tissues (i.e., scalp, skull, etc.) and the intracerebral part, in particular the brain cortex. Evaluations of changes in the absorption coefficients of each compartment at two wavelengths in the near-infrared region led us to separately assess ΔHbO_2 and ΔHb in the brain cortex and extracerebral tissues.

The diffuse reflectance Eq. (1) describes light propagation in the semi-infinitive homogenous medium as a function of time, t, and distance, ρ, between the source and the detector, assuming a delta Dirac light source pulse with absorption and diffusion coefficients that are homogenously distributed over the whole volume:[55]

$$R_h(\rho,t) = (\mu_s')^{-1}(4\pi Dc)^{-3/2}t^{-5/2}\,\exp\left(-\frac{\rho^2}{4Dct} - \mu_a ct\right), \tag{1}$$

where D is the diffusion coefficient ($D = [3(\mu_a + \mu_s')]^{-1}$), μ_a is the absorption coefficient of the medium, and μ_s' is the reduced scattering coefficient. Going further, we can assume the appearance of a change in the absorption coefficient, $\Delta\mu_a$, in a small inclusion of volume, dV, inside the medium in a location defined by vector r. It is possible to calculate time-dependent changes in the diffuse reflectance, $\Delta R(r,\rho,t)$, that are measured on the surface of the medium at source-detector separation, ρ, by the following equation:

$$\Delta R(r,\rho,t) = \Delta\mu_a dV[\phi(r,t) \otimes E(r,\rho,t)], \tag{2}$$

where function, Φ, is the time-dependent fluence rate of photons in the medium at location r and E is the escape function, which describes the probability that the photon emitted from location r will reach the detector at distance ρ from the source position.[54,56] By knowing the form of the function $R_h(1)$ and $\Delta R(2)$ we can derive the theoretical form of the diffusive reflectance, R_i, for the medium with the inclusion located at r:

$$R_i(r,\rho,t) = R_h(\rho,t) + \Delta R(r,\rho,t). \tag{3}$$

From the theoretical equations of diffuse reflectance, R_h and $R_i(r,\rho,t)$, we calculated the changes in the moments that occur after the appearance of absorption inclusion in the medium:

$$\Delta A_t = \frac{N_{\text{tot}i}}{N_{\text{tot}h}}, \tag{4}$$

$$\Delta\langle t\rangle_t = \langle t\rangle_i - \langle t\rangle_h, \tag{5}$$

$$\Delta V_t = V_i - V_h, \tag{6}$$

where the index, h, indicates moments of the theoretical DTOF calculated for the homogeneous medium and the index, i, indicates moments of theoretical DTOF calculated for the medium with a small absorption inclusion, $\Delta\mu_a$.

The theoretical model of the head that was adopted for our investigations consisted of 10 layers, each 0.3-cm thick [Fig. 3(a)]. On the surface of these layers, the distributions of the times of flights of the photons were collected in semi-infinite geometry. We assumed that the first three layers correspond to the extracerebral compartment and the layers from 6 to 10 represent the brain cortex [Fig. 3(a)]. Additionally, layers 4 and 5 were introduced to the analysis as a transition compartment that was considered in order to reduce crosstalk between the two main compartments during calculations. The above-described theoretical model of light propagation in the turbid media with the inclusion was utilized to determine the sensitivity factors of the moments of DTOFs [Fig. 3(b)].

The sensitivity factors of the three moments for each layer indexed by l are described as:

$$\text{MPP}_l = \frac{\Delta A_t}{\Delta\mu_{a,l}}, \tag{7}$$

$$\text{MTSF}_l = \frac{\Delta\langle t_t\rangle}{\Delta\mu_{a,l}}, \tag{8}$$

$$\text{VSF}_l = \frac{\Delta V_t}{\Delta\mu_{a,l}}, \tag{9}$$

where MPP_l is the mean partial path length, MTSF_l is the mean time of flight sensitivity factor, and VSF_l is the

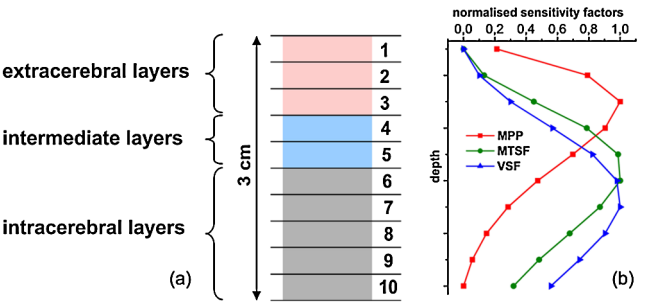

Fig. 3 Assumed model of a human head (a) where the layered model of the medium is represented by 10 theoretical homogeneous layers of the same thickness (0.3 cm) that are divided into three compartments: extracerebral, intermediate, and intracerebral and, corresponding to this model, the courses of the sensitivity factors of the moments of DTOFs as a function of depth (b). The mean partial path length (MPP), mean time of flight sensitivity factor (MTSF), and variance sensitivity factor (VSF) indicate the sensitivity of each moment (integral, mean time of flight, and variance, respectively) for absorption changes at the equivalent layer. It could be marked that variance is most sensitive to changes in the intracerebral compartment. The sensitivity factors of the moments of each compartment were calculated by summing MPP, MTSF, and VSF for the layers belonging to each corresponding compartment.

variance sensitivity factor, and $\Delta\mu_{a,l}$ is the change in the absorption coefficient in the layers indexed by l. In particular, the medium was divided into voxels of the size $0.33 \times 0.33 \times 0.33$ cm and changes in the moments ΔA_t, $\Delta\langle t\rangle_t$, and ΔV_t were calculated for inclusions that successively appear in each voxel. The sensitivity factor of each layer was obtained by integration of the voxels that corresponding to each particular layer.

Unfortunately, this method only allows us to calculate the sensitivity factors with the assumption that initially the medium was homogeneous, and it yields significant errors in the vicinity of the source and the detector positions. In order to provide the background optical properties for calculations of the sensitivity factors used for the analysis of the *in vivo* data, μ_a, μ_s', and $\Delta\mu_a$ were evaluated from the measurement of the DTOFs on the head of the subject before and after cross-clamping of the carotid artery, respectively. The method of the moments of the DTOFs[57] was used to obtain the optical properties of the medium with the assumption that the tissues under investigation were homogeneous.

The changes in the sensitivity factors as a function of depth are presented in Fig. 3(b). It is noted that variance is the most sensitive moment for changes of absorption coefficient in the deeper layers and the statistical moment, which is most sensitive to superficial changes in absorption and is the integral of the DTOF. The profiles of the sensitivity factors as a function of depth may depend on the wavelengths utilized. However, it was assumed that for both wavelengths used in the experiment the same profiles can be adopted. This method for calculating sensitivity factors was previously proposed and it was utilized in other trNIRS experiments, i.e., motor cortex stimulation[54] and monitoring the inflow of exogenous dye to brain tissue.[22,53]

The sensitivity factors of the moments for each compartment were calculated by summing up MPP, MTSF, and VSF of the layers of each corresponding compartment. Using the theoretically estimated sensitivity factors and the moments of the measured DTOFs, we evaluated changes in the absorption coefficient of all three compartments by solving the system of equations:

$$\begin{bmatrix} \mathrm{MPP}_1 & \mathrm{MPP}_2 & \mathrm{MPP}_3 \\ \mathrm{MTSF}_1 & \mathrm{MTSF}_2 & \mathrm{MTSF}_3 \\ \mathrm{VSF}_1 & \mathrm{VSF}_2 & \mathrm{VSF}_3 \end{bmatrix} \cdot \begin{bmatrix} \Delta\mu_{a,1} \\ \Delta\mu_{a,2} \\ \Delta\mu_{a,3} \end{bmatrix} = \begin{bmatrix} -\log(N_{\mathrm{tot}C}/N_{\mathrm{tot}0}) \\ \langle t\rangle_C - \langle t\rangle_0 \\ V_C - V_0 \end{bmatrix}, \tag{10}$$

where MPP_k, MTSF_k, and VSF_k correspond to the sensitivity factors of the moments summed for the extracerebral layers ($k = 1$, compartment 1), intermediate layers ($k = 2$, compartment 2), and intracerebral layers ($k = 3$, compartment 3); $\Delta\mu_{a,k}$ represents the unknown change of the absorption coefficient in each compartment; N_{tot}, $\langle t\rangle$, and V are the moments calculated from the measured DTOFs indexed by 0 and C, respectively, for the measurements taken before and after crossclamping of the carotid arteries.

The changes in the absorption coefficient obtained by solving Eq. (10) are related to the changes in concentration of $\Delta\mathrm{HbO}_2$ and $\Delta\mathrm{Hb}$ in each compartment:

$$\begin{bmatrix} \Delta\mu_{a,k}(\lambda_1) \\ \Delta\mu_{a,k}(\lambda_2) \end{bmatrix} = \ln(10) \cdot \begin{bmatrix} \varepsilon_{\mathrm{HbO2}}(\lambda_1) & \varepsilon_{\mathrm{Hb}}(\lambda_1) \\ \varepsilon_{\mathrm{HbO2}}(\lambda_2) & \varepsilon_{\mathrm{Hb}}(\lambda_2) \end{bmatrix} \cdot \begin{bmatrix} \Delta c_{\mathrm{HbO2},k} \\ \Delta c_{\mathrm{Hb},k} \end{bmatrix}, \tag{11}$$

where $\varepsilon_{\mathrm{HbO2}}$ and $\varepsilon_{\mathrm{Hb}}$ are the molar extinction coefficients of oxy and deoxyhemoglobin, respectively. The molar extinction coefficients were taken from spectra published by Wray et al.[21]

For every measured DTOF, background subtraction and correction for differential nonlinearity of the TCSPC electronics were performed. When calculating the moments, integration was carried out for the part of the DTOF in which the number of counts was larger than 1% of its maximum number of counts recorded in the every single DTOF.

3 Results

In Figs. 4 and 5, the time courses of oxy and deoxyhemoglobin for the extra and intracerebral compartments following crossclamping of the carotid arteries are presented. The results obtained for patient 1 (74-year-old man) during left carotid artery endarterectomy are presented in Fig. 4. The results obtained for patient 2 (71-year-old woman) during right carotid artery endarterectomy are presented in Fig. 5. Each panel corresponds to the 16 channels sampled on the ipsilateral and contralateral hemispheres (in respect to the side of the artery clamped), and it demonstrates the time courses of oxy and deoxyhemoglobin in the extra and intracerebral compartments. Markers M1 and M2 in Figs. 4 and 5 indicate the moment of crossclamping of the external carotid artery (ECA) and the internal carotid artery (ICA), respectively. Trends in the changes in hemoglobin concentrations presented in Figs. 4 and 5 were observed in the whole group of studied patients. It was noted that the crossclamping procedure caused a rapid decrease in the level of oxyhemoglobin in all source-detector pairs in both hemispheres in the extra as well as in the intracerebral compartments. However, these phenomena occurred on a larger scale in the ipsilateral hemisphere than in the contralateral hemisphere. It was also observed that the drop in oxyhemoglobin for the extracerebral layer occur before the intracerebral compartment. This effect is due to the delay between the moments of crossclamping ECA and ICA, as indicated by markers M1 and M2, respectively. This effect was observed in both patients in the ipsi and contralateral hemispheres. Similar changes are observed in the deoxyhemoglobin signal, but in this case the expected increase in the signal occurred after the arteries were clamped. The temporal reactions to the clamping procedure can be observed in more detail in Fig. 6 where the average signals for all measured positions on the ipsilateral hemispheres are presented for both patients.

Cross-clamping of ECA and ICA caused dynamic changes in oxy and deoxyhemoglobin, but after a few tens of seconds, stabilization of the signal was observed in all source-detector pairs (Figs. 4–6). The average values of the oxy- and deoxyhemoglobin changes observed after stabilization of both compartments in both hemispheres are compared in Table 1. It was also noted that the drop in the signal of the oxyhemoglobin concentration was faster in the intracerebral compartment than in the extracerebral compartment.

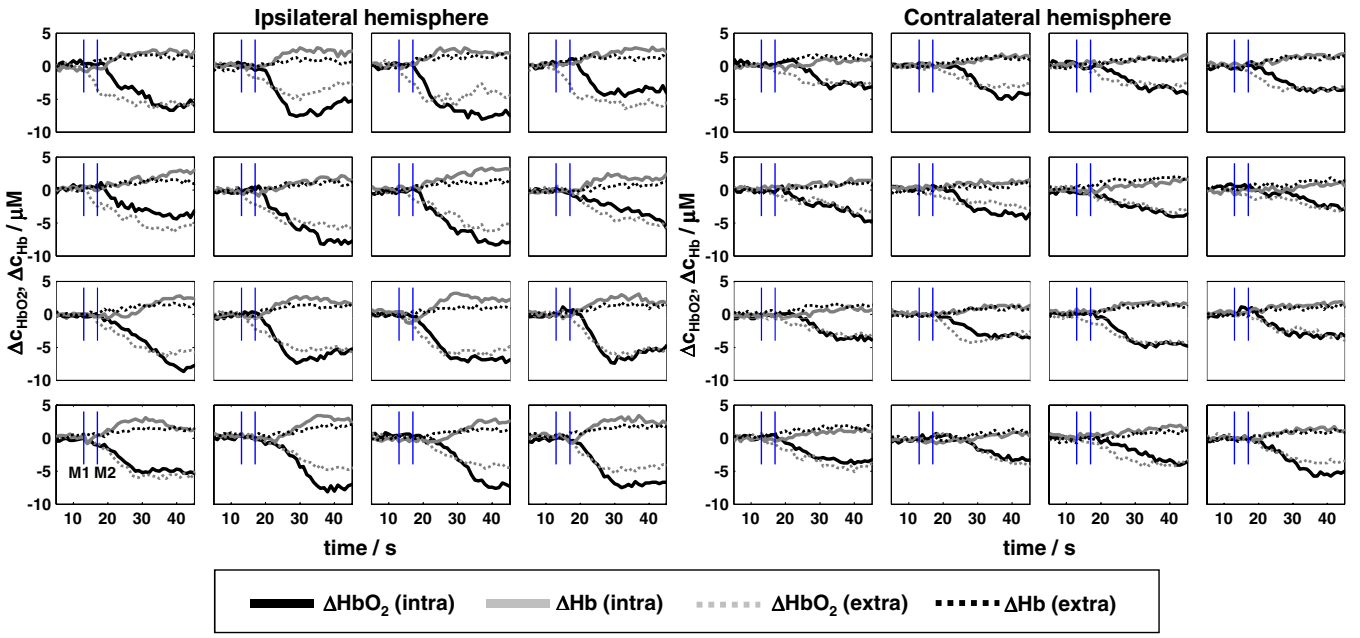

Fig. 4 Changes in oxy- and deoxyhemoglobin observed in patient 1. Markers M1 ($t = 13$ s) and M2 ($t = 17$ s) indicate cross-clamping of ECA and ICA, respectively. It should be noted that the drop in oxyhemoglobin in the ipsilateral hemisphere is larger than the drop in the contralateral hemisphere. Delay between the drop in the extracerebral ΔHBO2, which was crossclamped at $t = 13$ s, and the drop in intracerebral ΔHBO2, which was crossclamped at $t = 17$ s, can be observed. Similar but inverse effects were observed for deoxyhemoglobin in both hemispheres and the intra and extracerebral compartments.

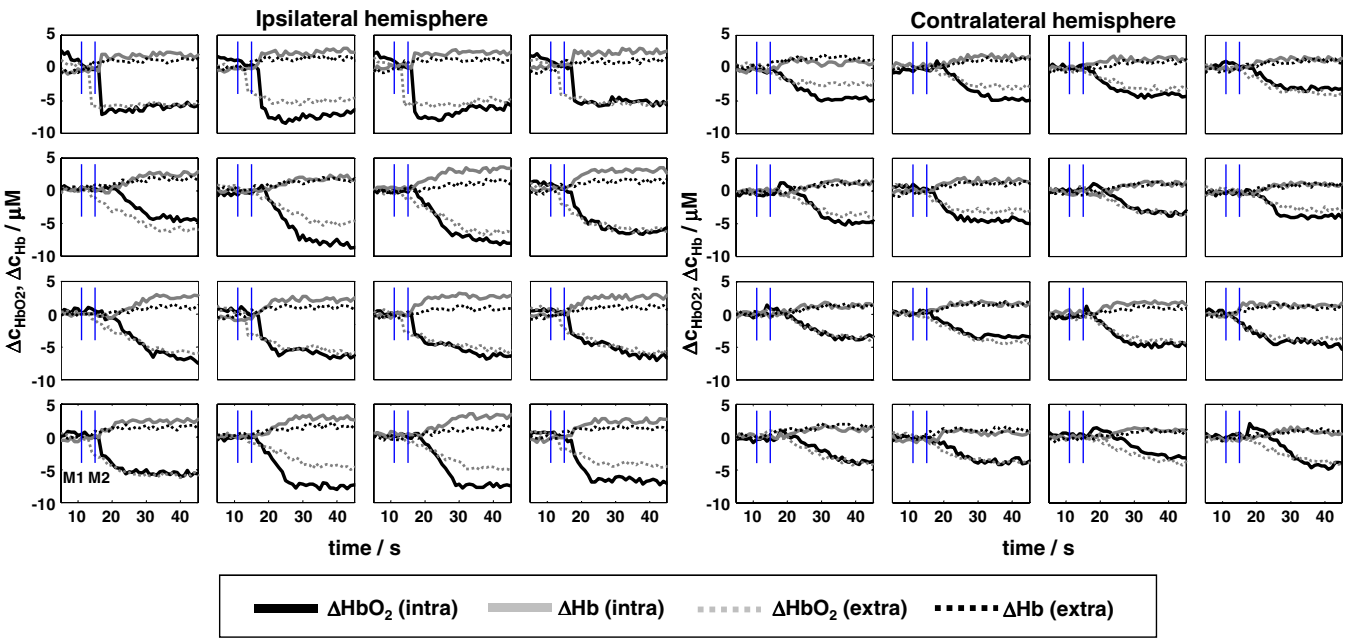

Fig. 5 Same as Fig. 4 but for patient 2. (M1 [$t = 11$ s] and M2 [$t = 15$ s]).

The time of stabilization, Δt_s, of the signal of Δc_{HbO2} after the cross-clamping of ICA and ECA was also analyzed. Δt_s was calculated to be the period between the time of cross-clamping of the artery, t_M, as indicated by the corresponding marker, M1 or M2, and the time, t_s, when the derivative of Δc_{HbO2} reaches 30% of signal in t_M. Δt_s can be given as $\Delta t_s = t_s - t_M$.

Due to the low signal-to-noise ratio and high movement artifacts observed in the vast majority of patients, the grand average was carried out of the selected signals from the whole group under investigation. The results obtained from the grand average are presented in Table 1. For the grand average procedure, changes in the oxy- and deoxyhemoglobin concentrations in the intra- and extracerebral layers of the 46 channels positioned on the ipsilateral hemisphere and 59 channels positioned on contralateral hemispheres were selected in 9 patients, including results from 2 patients presented in Figs. 4, 5, and 6. The signals

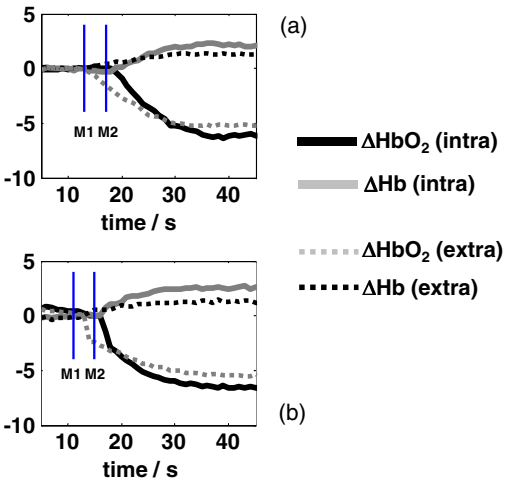

Fig. 6 Average signals of ΔHbO2 and ΔHb in the ipsilateral hemispheres of patients 1 (a) and 2 (b). Markers M1 and M2 indicate crossclamping of ECA and ICE, respectively. The time delay between the drop in the signal of ΔHbO2 in the extracerebral layer and the intracerebral compartment can be observed.

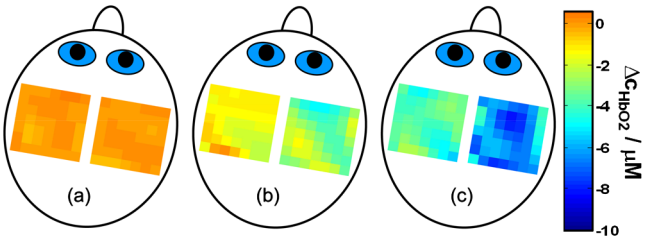

Fig. 7 Visualization of the changes in the oxyhemoglobin concentration on the surface of the brain cortex during (a) the initial stage of the surgery, (b) 3 s after crossclamping of ICA, and (c) stabilization stage 20 s after crossclamping of ICA.

recorded in the other eight patients were rejected due to very high noise and moving artifacts caused by difficult measurement conditions.

Channels for the grand average were selected by manually checking all signals from the whole group of patients. If Δc_{HbO2} decreased and Δc_{Hb} increased after cross-clamping of the corresponding artery in both the intra- and extracerebral layers of the selected channel, the signal was used in the grand average procedure.

The visualization of changes in oxyhemoglobin on the surface of the brain cortex for patient 1 is presented in Fig. 7. The maps of the three time intervals were recalculated for both hemispheres. In Fig. 7(a), the initial level of $\Delta\mathrm{HbO}_2$, before crossclamping of ICA, is presented, which was calculated 5 s before crossclamping of ECA. In Fig. 7(b), a decreasing concentration level was observed as a consequence of the ICA crossclamping. Figure 7(c) illustrates the spatial distribution of the oxyhemoglobin concentration on the surface of the brain cortex 20 s after crossclamping of the intracerebral carotid artery. It can be observed that the dynamics of the drop in the concentration of $\Delta\mathrm{HbO}_2$ is spatially homogeneous in the area that was imaged using the trNIRS technique. For a better representation, the measured maps were interpolated from the size 4×4 to 7×7 using the 2-D data interpolation function of the Matlab package (Mathworks, USA).

4 Discussion and Conclusions

Application of the constructed time-resolved optical brain imager for monitoring brain oxygenation during carotid endarterectomy is presented. This paper is a first report on the use of a time-resolved technique in combination with multichannel measurements during crossclamping of the carotid arteries in the operating room. Our results could be also beneficial for the further development of monitoring methodology to assess brain oxygenation in patients during carotid surgery because by using this technique we were able to assess oxygenation of the tissue of the head with depth discrimination.[30,53] Thus, the influence of the skin and the extracerebral tissue can be omitted during monitoring of brain hemodynamics.[36,58,59]

Monitoring of brain hemodynamics during cross-clamping of the carotid artery revealed distinct changes in the concentration of oxy- and deoxyhemoglobin in the brain cortex. The observed variations in brain oxygenation were similar in each source-detector pair. These phenomena may suggest that effective monitoring of brain oxygenation during carotid artery surgery could be routinely carried out by single-channel measurement with a device much simpler than our trNIRS imaging system. This problem has also been discussed by other authors.[31]

It was observed that the drop in the signal in the ipsilateral hemisphere was more significant than the drop the contralateral

Table 1 Comparison of changes in the concentrations of oxy- and deoxyhemoglobin in the intra- and extracerebral tissue compartments on both sites of the head and the results of the grand average procedure for chosen optodes in the whole group of the patients.

		Patient 1			Patient 2			Whole group (selected optodes)		
		$\Delta\mathrm{HbO}_2/\mu\mathrm{M}$	$\Delta\mathrm{Hb}/\mu\mathrm{M}$	$\Delta t_s/s$	$\Delta\mathrm{HbO}_2/\mu\mathrm{M}$	$\Delta\mathrm{Hb}/\mu\mathrm{M}$	$\Delta t_s/s$	$\Delta\mathrm{HbO}_2/\mu\mathrm{M}$	$\Delta\mathrm{Hb}/\mu\mathrm{M}$	$\Delta t_s/s$
Ipsilatreal	Intracerebral	−6.3	2.2	18	−6.6	1.3	20	-5.9 ± 1.5	1.3 ± 0.3	20 ± 3
	Extracerebral	−5.1	1.3	22	−5.5	2.4	25	-4.5 ± 1.1	2.0 ± 1.2	25 ± 4
Contralateral	Intracerebral	−4.0	1.0	21	−4.1	1.3	25	-4.2 ± 1.8	1.6 ± 0.6	26 ± 3
	Extracerebral	−3.3	1.2	23	−3.6	1.3	30	-3.0 ± 1.3	1.2 ± 0.5	27 ± 2

hemisphere, which can be explained by brain hemodynamics and anatomy. The observed effect on the oxygenation signals in the contralateral site of the head suggests that in the monitored patients the ipsilateral hemisphere was supplied by the contralateral and vertebral arteries through the circle of Willis.[60]

The obtained results are also very interesting from the point of view of optical measurement methodology. This is the first report that a timeresolved optical imager equipped with 2 wavelengths, 32 emitting fibers, and 8 independent detection channels can be used during the clamping of carotid arteries, which could be a very good model for depth-resolved analysis. As it is shown in Figs. 4, 5, and 6, the previously proposed signal-processing methods[30,53,54] enable the separation of changes in the concentrations of oxy- and deoxyhemoglobin in the extra- and intracerebral compartments. The delay between moments of reaction in the oxygenation signals obtained from the intra- and extracerebral compartments is clearly visible in Fig. 6. This delay reflects the sequence of cross-clamping the ECA and ICA, which mostly supply the extra- and intracerebral tissue compartments, respectively.

In our setup, a single map of the oxy- and deoxyhemoglobin concentration changes from both hemispheres was obtained within about 1 s. This sampling frequency enables the measurement of rapid changes in oxygenation and is near the sampling frequency used in commercial non-timeresolved devices.

The introduction of a brain imager into the operating room was relatively easy, considering the limited space available in the operating room and the presence of other standard equipment necessary for surgeries. The trNIRS device was constructed on a transportable trolley in a cabinet measuring $60 \times 60 \times 140$ cm. During the surgery, it was positioned next to the patient's head, so access to the patient's head was limited because three members of the surgical team required access to the relatively small operation area. Measurements were carried out using the large holder with the emitting fibers and detecting fiber bundles. This rather heavy setup was placed very near to the operating field around the patient's head. An additional obstacle in NIRS measurements is the fact that the operating field is very intensively illuminated. This illumination could result in a decrease in the signal-to-noise ratio and is dangerous for sensitive photomultipliers tubes that could be destroyed by accidental over-illumination. For the measurement procedure, two people were necessary: the control software operator and the assistant responsible for fixing the fiber holder cap to the defined position on the head during the critical moment of the surgery. Because of the fact that during the whole operation the patients were kept conscious and the surgical field was located close in respect to the measurement site, the recorded signals were usually unstable with large movement artifacts.[61] In fact, many of the recorded signals could not be analyzed because of low quality, high level of noise, and motion artifacts. In many cases, a good quality signal appeared only in several channels, but only in two of the cases we were able to properly register the entire constellation of changes in the concentrations of oxy- and deoxyhemoglobin. A reduction in the number of emitting fibers and detecting fiber bundles may reduce the problem of movement artifacts because mounting the optode holder on the head would be easier. However, this solution would lead to reduction in the size of the monitored area of the brain.

Although carotid endarterectomy remains the "gold standard" treatment for carotid stenosis, carotid stenting and angioplasty are also frequently performed.[62–64] In selected patients with acute cerebral artery thrombosis, one can offer direct thrombolysis with or without endovascular procedures. In all possible extra- and intracerebral vascular procedures, an objective measurement technique and adequate equipment for brain oxygenation monitoring is expected to detect and recognize on-line deficits in cerebral blood perfusion caused by thrombosis or embolization. This remains essential to prevent and properly cure neurological disturbances that may occur during vascular procedures.

Despite some technical problems mentioned above, we can conclude that the proposed optical method for intraoperative imaging of brain hemodynamics is feasible for brain oxygenation monitoring in all carotid vascular procedures performed in clinical practice.

Our results provide a good perspective for the future application of the trNIRS technique during endarterectomy surgery. The observed homogeneity of brain oxygenation changes after crossclamping of the arteries leads us to the conclusion that the number of time-resolved channels can be reduced for this particular application and, consequently, the size of the fiber holder and the whole instrument itself can be reduced. This reduction may facilitate continuous brain-specific monitoring of tissue oxygenation during the whole carotid vascular surgery.

Acknowledgments

The research leading to these results received funding from the European Community's Seventh Framework Programme (FP7/2007-2013) under grant agreement #201076. The study was also partly financed by research project #3T11E00627 that was financed by the Polish Ministry of Science and Higher Education.

References

1. NASCET collaborators, "Beneficial effect of carotid endarterectomy in symptomatic patients with high-grade carotid stenosis," *N. Engl. J. Med.* **325**(7), 445–453 (1991).
2. R. Maharaj, "A review of recent developments in the management of carotid artery stenosis," *J. Cardiothorac. Vasc. Anesth.* **22**(2), 277–289 (2008).
3. C. D. Liapis et al., "ESVS guidelines. Invasive treatment for carotid stenosis: indications, techniques," *Eur. J. Vasc. Endovasc. Surg.* **37**(4 Suppl.), 1–19 (2009).
4. F. Guarracino, "Cerebral monitoring during cardiovascular surgery," *Curr. Opin. Anaesthesiol.* **21**(1), 50–54 (2008).
5. R. Mofidi et al., "Angiogenesis in carotid atherosclerotic lesions is associated with timing of ischemic neurological events and presence of computed tomographic cerebral infarction in the ipsilateral cerebral hemisphere," *Ann. Vasc. Surg.* **22**(2), 266–272 (2008).
6. M. M. Tedesco et al., "Postprocedural microembolic events following carotid surgery and carotid angioplasty and stenting," *J. Vasc. Surg.* **46**(2), 244–250 (2007).
7. M. Uno et al., "Hemodynamic cerebral ischemia during carotid endarterectomy evaluated by intraoperative monitoring and postoperative diffusion-weighted imaging," *Neurol. Res.* **29**(1), 70–77 (2007).
8. K. Aso et al., "Preoperative cerebrovascular reactivity to acetazolamide measured by brain perfusion SPECT predicts development of cerebral ischemic lesions caused by microemboli during carotid endarterectomy," *Eur. J. Nucl. Med. Mol. Imaging* **36**(2), 294–301 (2009).

9. M. Skjelland et al., "Cerebral microemboli and brain injury during carotid artery endarterectomy and stenting," *Stroke* **40**(1), 230–234 (2008).
10. G. Mommertz et al., "Early control of distal internal carotid artery during carotid endarterectomy does it reduce cerebral microemboli?," *J. Cardiovasc. Surg.* (Torino) **51**(3), 369–375 (2009).
11. M. Collice et al., "Role of EEG monitoring and cross-clamping duration in carotid endarterectomy," *J. Neurosurg.* **65**(6), 815–819 (1986).
12. A. B. Baker and A. J. Roxburgh, "Computerised EEG monitoring for carotid endarterectomy," *Anaesth. Intensive Care* **14**(1), 32–36 (1986).
13. S. Fielmuth and T. Uhlig, "The role of somatosensory evoked potentials in detecting cerebral ischaemia during carotid endarterectomy," *Eur. J. Anaesthesiol.* **25**(8), 648–656 (2008).
14. J. M. Guerit et al., "Somatosensory evoked potential monitoring in carotid surgery. I. Relationships between qualitative SEP alterations and intraoperative events," *Electroencephalogr. Clin. Neurophysiol.* **104**(6), 459–469 (1997).1
15. P. De Vleeschauwer, S. Horsch, and R. Matamoros, "Monitoring of somatosensory evoked potentials in carotid surgery: results, usefulness and limitations of the method," *Ann. Vasc. Surg.* **2**(1), 63–68 (1988).
16. W. F. Haupt and S. Horsch, "Evoked potential monitoring in carotid surgery: a review of 994 cases," *Neurology.* **42**(4), 835–838 (1992).
17. F. F. Jobsis, "Noninvasive, infrared monitoring of cerebral and myocardial oxygen sufficiency and circulatory parameters," *Science* **198**(4323), 1264–1267 (1977).
18. A. Villringer and B. Chance, "Non-invasive optical spectroscopy and imaging of human brain function," *Trends Neurosci.* **20**(10), 435–442 (1997).
19. G. Litscher and G. Schwarz, "Transcranial Cerebral Oximetry," Pabst. Sci. Pub., Lengerich (1997).
20. H. Obrig and A. Villringer, "Beyond the visible: imaging the human brain with light," *J. Cereb. Blood Flow Metab.* **23**(1), 1 (2003).
21. S. Wray et al., "Characterization of the near infrared absorption spectra of cytochrome aa3 and haemoglobin for the non-invasive monitoring of cerebral oxygenation," *Biochim. Biophys. Acta.* **933**(1), 184–192 (1988).
22. A. Liebert et al., "Bed-side assessment of cerebral perfusion in stroke patients based on optical monitoring of a dye bolus by time-resolved diffuse reflectance," *Neuroimage* **24**(2), 426–435 (2005).
23. D. M. Hueber et al., "Non-invasive and quantitative near-infrared haemoglobin spectrometry in the piglet brain during hypoxic stress, using a frequency-domain multidistance instrument," *Phys. Med. Biol.* **46**(1), 41–62 (2001).
24. P. G. Al-Rawi, P. Smielewski, and P. J. Kirkpatrick, "Preliminary evaluation of a prototype spatially resolved spectrometer," *Acta. Neurochir. Suppl.* **71**, 255–257 (1998).
25. T. Tu et al., "Analysis on performance and optimization of frequency-domain near-infrared instruments," *J. Biomed. Opt.* **7**(4), 643–649 (2002).
26. A. Kienle and M. S. Patterson, "Determination of the optical properties of semi-infinite turbid media from frequency-domain reflectance close to the source," *Phys. Med. Biol.* **42**(9), 1801–1819 (1997).
27. B. W. Pogue and M. S. Patterson, "Frequency-domain optical absorption spectroscopy of finite tissue volumes using diffusion theory," *Phys. Med. Biol.* **39**(7), 1157–1180 (1994).
28. R. Cubeddu et al., "Time-resolved imaging on a realistic tissue phantom: mu(s)' and mu(a) images versus time-integrated images," *Appl. Optics* **35**(22), 4533–4540 (1996).
29. P. Taroni et al., "Time-resolved spectroscopy and imaging in diffusive media applied to medical diagnostics," *Riv. Nuovo Cimento.* **25**(4), 1–19 (2002).
30. J. Steinbrink et al., "Determining changes in NIR absorption using a layered model of the human head," *Phys. Med. Biol.* **46**(3), 879–896 (2001).
31. C. W. Pennekamp et al., "The value of near-infrared spectroscopy measured cerebral oximetry during carotid endarterectomy in perioperative stroke prevention: a review," *Eur. J. Vasc. Endovasc. Surg.* **38**(5), 539–545 (2009).
32. W. Staszkiewicz et al., "Use of transcranial cerebral oximetry in carotid surgery," *Polski Przegląd Chirurgiczny* **73**(2), 186–199 (2001).
33. R. Maniewski et al., "Near infrared spectroscopy for monitoring of cerebral oxygenation during carotid surgery," *Technol. Health Care* **9**(1–2), 181–183 (2001).
34. P. G. Al-Rawi and P. J. Kirkpatrick, "Tissue oxygen index: thresholds for cerebral ischemia using near-infrared spectroscopy," *Stroke* **37**(11), 2720–2725 (2006).
35. U. Beese et al., "Comparison of near-infrared spectroscopy and somatosensory evoked potentials for the detection of cerebral ischemia during carotid endarterectomy," *Stroke* **29**(10), 2032–2037 (1998).
36. J. A. de Letter et al., "Near-infrared reflected spectroscopy and electroencephalography during carotid endarterectomy: in search of a new shunt criterion," *Neurol. Res.* **20**(Suppl 1), S23–27 (1998).
37. C. M. Duffy et al., "Comparison of cerebral oximeter and evoked potential monitoring in carotid endarterectomy," *Can. J. Anaesth.* **44**(10), 1077–1081 (1997).
38. G. Grubhofer et al., "Comparing Doppler ultrasonography and cerebral oximetry as indicators for shunting in carotid endarterectomy," *Anesth. Analg.* **91**(6), 1339–1344 (2000).
39. O. Hirofumi et al., "The effectiveness of regional cerebral oxygen saturation monitoring using near-infrared spectroscopy in carotid endarterectomy," *J. Clin. Neurosci.* **10**(1), 79–83 (2003).
40. P. J. Kirkpatrick et al., "An observational study of near-infrared spectroscopy during carotid endarterectomy," *J. Neurosurg.* **82**(5), 756–763 (1995).
41. P. F. Mason et al., "The assessment of cerebral oxygenation during carotid endarterectomy utilising near infrared spectroscopy," *Eur. J. Vasc. Surg.* **8**(5), 590–594 (1994).
42. S. Moritz et al., "Accuracy of cerebral monitoring in detecting cerebral ischemia during carotid endarterectomy: a comparison of transcranial Doppler sonography, near-infrared spectroscopy, stump pressure, and somatosensory evoked potentials," *Anesthesiology* **107**(4), 563–569 (2007).
43. S. Nakamura et al., "Optical topography can predict occurrence of watershed infarction during carotid endarterectomy: technical case report," *Surg. Neurol.* **71**(5), 540–542 (2009).
44. A. Rigamonti et al., "A clinical evaluation of near-infrared cerebral oximetry in the awake patient to monitor cerebral perfusion during carotid endarterectomy," *J. Clin. Anesth.* **17**(6), 426–430 (2005).
45. P. Vets et al., "Cerebral oximetry in patients undergoing carotid endarterectomy: preliminary results," *Acta. Anaesthesiol. Belg.* **55**(3), 215–220 (2004).
46. I. M. Williams et al., "Light-reflective cerebral oximetry and jugular bulb venous oxygen saturation during carotid endarterectomy," *Br. J. Surg.* **81**(9), 1291–1295 (1994).
47. I. M. Williams et al., "Cerebral oxygen saturation, transcranial Doppler ultrasonography and stump pressure in carotid surgery," *Br. J. Surg.* **81**(7), 960–964 (1994).
48. K. Yamamoto, T. Miyata, and H. Nagawa, "Good correlation between cerebral oxygenation measured using near infrared spectroscopy and stump pressure during carotid clamping," *Int. Angiol.* **26**(3), 262–265 (2007).
49. K. Ogasawara et al., "Transcranial regional cerebral oxygen saturation monitoring during carotid endarterectomy as a predictor of postoperative hyperperfusion," *Neurosurgery* **53**(2), 309–314, discussion 314-305 (2003).
50. P. J. Kirkpatrick et al., "Defining thresholds for critical ischemia by using near-infrared spectroscopy in the adult brain," *J. Neurosurg.* **89**(3), 389–394 (1998).
51. A. Liebert et al., "Fiber dispersion in time domain measurements compromising the accuracy of determination of optical properties of strongly scattering media," *J. Biomed. Opt.* **8**(3), 512–516 (2003).
52. H. Wabnitz et al., "A time-domain NIR brain imager applied in functional stimulation experiments," *Proc. SPIE* (2005).
53. A. Liebert et al., "Time-resolved multidistance near-infrared spectroscopy of the adult head: intracerebral and extracerebral absorption changes from moments of distribution of times of flight of photons," *Appl. Opt.* **43**(15), 3037–3047 (2004).
54. M. Kacprzak et al., "Time-resolved optical imager for assessment of cerebral oxygenation," *J. Biomed. Opt.* **12**(3), 034019 (2007).
55. M. S. Patterson, B. Chance, and B. C. Wilson, "Time resolved reflectance and transmittance for the non/invasive measurement of tissue optical properties," *Appl. Opt.* **28**, 2331–2336 (1989).

56. M. Patterson and B. Pogue, "Mathematical model for time-resolved and frequency-domain fluorescence spectroscopy in biological tissues," *Appl. Opt.* **33**, 1963–1974 (1994).
57. A. Liebert et al., "Evaluation of optical properties of highly scattering media by moments of distributions of times of flight of photons," *Applied Optics* **42**(28), 5785–5792 (2003).
58. C. Whiten and P. Gunning, "Carotid endarterectomy: intraoperative monitoring of cerebral perfusion," *Current Anaesthesia & Critical Care* **20**, 42–45 (2009).
59. S. Kuroda et al., "Near-infrared monitoring of cerebral oxygenation state during carotid endarterectomy," *Surg. Neurol.* **45**(5), 450–458 (1996).
60. D. O. Quest, "Stroke: a selective history," *Neurosurgery* **27**(3), 440–445 (1990).
61. R. Maniewski et al., "Near infrared spectroscopy for monitoring of cerebral oxygenation during carotid surgery," *Technol. and Health Care* **9**(1–2), 181–183 (2001).
62. A. I. Qureshi et al., "Carotid angioplasty with or without stent placement versus carotid endarterectomy for treatment of carotid stenosis: a meta-analysis," *Neurosurgery* **56**(6), 1171–1179, discussion 1179–1181 (2005).
63. M. H. Murad et al., "Endarterectomy vs stenting for carotid artery stenosis: a systematic review and meta-analysis," *J. Vasc. Surg.* **48**(2), 487–493 (2008).
64. J. Golledge, "Carotid stenting or endarterectomy for stroke prevention," *Med. J. Aust.* **176**(3), 134–135 (2002).